no TGF-β1 dimers are secreted from cells transfected with the plasmid pPTH-TGF (Fig. 2B, lane 7), cotransfection of pPTH-TGF and pProTGF results in secretion of biologically active TGF-β1 dimers (Fig. 2B, lane 9, and Table 1). As judged by bioactivity and ELISA, ~2.4% of the amount of TGF-β1 present in supernatants from pTGF-β–transfected cells was present in supernatants from pPTH-TGF and pProTGF-transfected cells (Table 1). The reasons for the lower efficiency of dimer rescue by the proTGF-β sequence as compared with the results obtained with the activin A constructions are not understood.

No activin A dimers were secreted from cells transfected with pPTH-A and pProTGF, but activin A dimers were detected in transfection experiments with a vector containing the proTGF-β1 sequences fused to the mature activin A sequences (*6*). It would therefore appear that the proTGF-β1 sequences can substitute, albeit at a low efficiency, for the activin A pro-sequences. This result suggests that sequences in the pro-region responsible for mature region–pro-region interaction may be conserved between activin A and TGF-β1. The pro-region of TGF-β1 has been shown to contain one or more binding sites for the mature homodimers since the pro-regions and mature regions are secreted from cells as a large noncovalently linked latent complex (*7*). It is tempting to speculate that the binding site or sites responsible for the formation of the TGF-β1 noncovalent complex are also used by the pro-region as it aids the dimerization of the mature regions.

The results of the complementation experiments presented here demonstrate that the pro-regions of activin A and TGF-β1 are essential for the folding and assembly of activin A and TGF-β1 dimers. The ability of an independently expressed pro-region to aid in the folding of a mature protein has been previously reported for a number of proteases (*8*).

REFERENCES AND NOTES

1. J. Massagué, *Cell* **49**, 437 (1987).
2. A. J. Mason *et al.*, *Nature* **318**, 659 (1985).
3. R. Derynck *et al.*, *ibid.* **316**, 701 (1985).
4. R. H. Schwall, K. Nikolics, E. Szonyi, C. Gorman, A. J. Mason, *Mol. Endocrinol.* **3**, 1237 (1988).
5. G. N. Hendy, H. M. Kronenberg, J. T. Potts, Jr., A. Rich, *Proc. Natl. Acad. Sci. U.S.A.* **78**, 7365 (1981).
6. A. M. Gray and A. J. Mason, unpublished data.
7. L. E. Gentry, M. N. Liubin, A. F. Purchio, H. Marquardt, *Mol. Cell. Biol.* **8**, 4162 (1988); K. Miyazono, V. Hellman, C. Wernstadt, C.-H. Heldin, *J. Biol. Chem.* **263**, 7646 (1988).
8. X. Zhu, Y. Ohta, F. Jordan, M. Inouye, *Nature* **339**, 483 (1989); J. L. Silen and D. A. Agard, *ibid.* **341**, 462 (1989).
9. W. Vale, G. Grant, M. Amoss, R. Blackwell, R. Guillemin, *Endocrinology* **91**, 562 (1972).
10. L. M. Wakefield, D. M. Smith, K. C. Flanders, M. B. Sporn, *J. Biol. Chem.* **263**, 7646 (1988).
11. C. M. Gorman, D. R. Gies, G. McCray, *DNA-Protein Eng.* **2**, 1 (1990).
12. The sequences coding for the mature activin A subunit in pActA were assembled from synthetic oligonucleotides, a procedure that introduced unique restriction sites but conserved the protein sequence. pProA: To express the prepro-polypeptide of the activin A precursor, a stop codon was introduced in pActA. The Xba I site was filled in generating a stop codon five amino acids downstream from the basic processing site of the propeptide and creating the sequence Gly-Leu-Ala-Arg-Val after Arg^{282}. The Cla I–Hinc II fragment was then recloned into the vector RKB that had been cut with Cla I and Sma I. pPTH-A: A synthetic 113-bp Eco RI–Xba I fragment encoding the PTH prepro-polypeptide fused to the first three bases of mature activin A sequences was ligated into the plasmid pActA that had been cut with Eco RI and Xba I, replacing the βA prepro-sequences. pProTGF: A stop codon was introduced after Ser^{276} of the TGF-β propeptide, deleting the basic cleavage site, by ligation of a synthetic 21-bp Apa I–Hind II fragment and the 817-bp Eco RI–Apa I fragment from pTGF-β into the vector pRK5 that had been cut with Eco RI and Hind II. pPTH-TGF: A synthetic 113-bp Eco RI–Ban II fragment encoding the PTH prepro-polypeptide fused to the first three bases of mature TGF-β sequences was ligated along with the 96-bp Ban II–Bam HI fragment from pTGF-β into the plasmid pTGF-β that had been cut with Eco RI and Bam HI.
13. F. L. Graham and A. J. van der Eb, *Virology* **52**, 456 (1973).
14. C. Gorman, R. Padmanabhan, B. H. Howard, *Science* **221**, 551 (1983).
15. Human 293S cells seeded at ~30% confluency in 60-mm dishes were transfected the following day with 2.5 μg of each plasmid DNA and 2 μg of plasmid encoding the SV40 T-antigen and the Rous sarcoma virus promoter. The next day cells were labeled in 1.0 ml of serum-free Dulbecco's minimum essential medium with [^{35}S]cysteine and [^{35}S]methionine (250 μCi/ml each) for 1 to 2 hours. Labeling medium was removed, and secreted proteins were collected for 4 to 5 hours in 1 ml of serum-free medium. The supernatant was cleared by centrifugation, and rinsed cells were lysed in 0.5 ml of lysis buffer (1% NP-40, 0.5% deoxycholate, 0.1% SDS; and 5 m*M* EDTA in phosphate-buffered saline) and spun for 10 min, and the lysate was frozen until use. Secreted proteins (100 μl) were immunoprecipitated with either polyclonal antibody 290B, an antibody to recombinant human activin A dimer that recognizes both dimer and monomer (and displays some cross-reaction with the activin A precursor sequences), or mouse MAb 2G7 to recombinant human TGF-β. Cell lysates were immunoprecipitated with MAb 309, which recognizes only activin A dimer. Supernatants to be precipitated with the TGF-β antibody were heated at 75°C for 5 min in the presence of 0.1% bovine serum albumin and chilled on ice before addition of antibody. Immune complexes of secreted proteins were precipitated with Pansorbin (Calbiochem) and cell lysates, with protein A–Sepharose (Pharmacia). Denatured immunoprecipitates or total secreted proteins (15 μl) were separated by electrophoresis on 13% SDS-polyacrylamide gels and were permeated with Enhance (Du Pont) and exposed for 3 days at ~70°C.

16. We thank A. Evans for critical comments on this manuscript; A. Levinson and S. Broz for supplying the plasmid pTGF-β (SBβ); H. Niall for the suggestion of using the prepro-region of PTH; and R. Schwall, W.-L. Wong, J. Lofgren, L. Bald, and members of the Genentech assay group for assistance. Synthetic oligonucleotides were made by P. Ng, M. Vasser, and P. Jhurani of the Genentech DNA synthesis group.

10 October 1989; accepted 12 January 1990

Imaging and Manipulating Molecules on a Zeolite Surface with an Atomic Force Microscope

A. L. WEISENHORN, J. E. MAC DOUGALL, S. A. C. GOULD, S. D. COX, W. S. WISE, J. MASSIE, P. MAIVALD, V. B. ELINGS, G. D. STUCKY, P. K. HANSMA

The adsorption of neutral molecules and ions on the surfaces of zeolites was observed in real time with an atomic force microscope (AFM). Direct imaging of the surface of the zeolite clinoptilolite was possible by using a diluted *tert*-butyl ammonium chloride solution as a medium. Images of the crystal in different liquids revealed that molecules could be bound to the surface in different ways; neutral molecules of *tert*-butanol formed an ordered array, whereas *tert*-butyl ammonium ions formed clusters. These absorbed molecules were not rearranged by the AFM tip when used in an imaging mode. However, when a sufficiently large force was applied, the tip of the AFM could rearrange the *tert*-butyl ammonium ions on the zeolite surface. This demonstration of molecular manipulation suggests new applications, including biosensors and lithography.

ZEOLITES ARE CRYSTALLINE ALUminosilicates that have a regular pore or channel structure on the order of atomic dimensions (*1*). Introducing aluminum atoms into a silica network yields a negative charge per Al atom so that cations are required to balance the charge. These cations are loosely bound to framework oxygen atoms and can be readily exchanged for other cations in most cases. Zeolites with the appropriate combination of molecularly sized holes and cation exchange ability have found a great number of uses in the chemical industry. For example, acid zeolite Y catalysts are used to crack crude oil (*2*), ZSM-5 (a high silica content zeolite) is used to convert methanol to gasoline (*3*), zeolite A is used as a water softener in homes (*4*), and clinoptilolite is used for waste-water treatment to remove ammonium and phosphate

ions (*5*). To understand how molecules or cations interact with the framework of zeolites, scientists have used a vast number of techniques ranging from x-ray crystallography to solid-state nuclear magnetic resonance (NMR) and electron microscopy (*6*). Most of these techniques give complementary information about how the zeolite and the molecule change as the two interact. However, imaging the real-time interactions of molecules or cations with a zeolite surface has not been possible with molecular resolution. The AFM offers such an opportunity.

Previously, AFMs (*7*) have been used to nondestructively image insulating surfaces with atomic resolution (*8*) even at 4 K (*9*) and in vacuum (*10*). Polymers (*11*), amino acid crystal (*12*), and the magnetic domains in a thin film of a cobalt alloy (*13*) have been imaged with AFMs, and AFMs have also been used for atomic-scale friction measurements (*14*) and for the deposition and measurement of localized charges (*15*). Furthermore, AFMs can image soft surfaces such as cells (*16*) and other biological samples (*17, 18*) in water, because they can image with nondestructive forces as small as 1 nN (*19*).

This report details the use of an AFM to image the surface of a clinoptilolite crystal in various media and under different conditions. We show direct imaging of the crystal surface, adsorption of *tert*-butanol onto the crystal, the clustering of *tert*-butyl ammonium cations [$H_3NC(CH_3)_3^+$], and molecular manipulation, or lithography, on an adsorbed layer of the cations.

A natural crystal of clinoptilolite (*20*) (1.9 mm by 1.2 mm by 0.5 mm) from Succor Creek, Oregon, was used initially without any chemical modification. The crystal was glued with epoxy onto a stainless steel plate, cleaved with a scalpel parallel to the (010) plane, and mounted in the AFM (see Fig. 1). The crystal was imaged under different liquids, which were introduced by filling a sealed cell (see lower schematic of Fig. 1). The images were collected with Nanoscope II electronics and software (*21*) 20 min after exposure to allow an equilibrium state to be reached. Each image was acquired in either 2.5 or 10 s.

Direct imaging by the AFM of the surface of the crystal clinoptilolite (*22, 23*) [see Fig. 2A for the geometry of its tetrahedral framework (*24*)] was performed by first cleaning it in a 0.1*M* NaOH aqueous solution at about 60°C for 1 hour to remove organic residues. The crystal was then reglued to the stainless steel plate and put into the AFM. Next, the sealed cell was filled with 0.05*M* *tert*-butyl ammonium chloride solution (1:1 water:methanol). This solution was chosen because the *tert*-butyl ammonium cations are larger than the 8-ring pores of the crystal, which prevents the cations from going into these pores (the ring size is the number of aluminate and silicate units). Methanol was added to the aqueous *tert*-butyl ammonium chloride solution to break up the water structure (*25*). Finally, the crystal was rinsed in the cell with deionized water and the surface was imaged (Fig. 2B). The measured lattice spacings in Fig. 2B are 0.75, 0.86, and 0.83 nm with correct angles between the directions (compare with inset of Fig. 2B).

Since zeolites are used for filtering and adsorption, it was natural to attempt to image the adsorption of molecules onto the surface of the crystal clinoptilolite. The neutral compound *tert*-butanol (*26*) was chosen for the adsorption because of its size and its structure (polar OH group connected to apolar *tert*-butyl group). Again, the size prevents these molecules from entering the 8-ring pores. The *tert*-butanol was injected into the sealed cell on top of a freshly cleaved crystal surface.

The AFM image of the crystal surface (010) in *tert*-butanol is shown in Fig. 2C. The monolayer of *tert*-butanol molecules forms an ordered array, which suggests that the *tert*-butanol is absorbed into the 8-rings with its OH group pointing down into the pore. This orientation would offer some additional coordination to the cations in the pores. Distances calculated from crystal structure (*27*) agree with the distances in the image; repeat distances in the image were 0.87 nm (in the +32° direction, measured from the positive *x*-axis counterclockwise), 0.92 nm (+80°), and 0.74 nm (+140°), which corresponds to the distance from center to center of the 8-rings within the estimated error of ≲10% due to the drift and other uncertainties of the AFM and crystal variation by hydration. Diffusion and therefore the exchange of the *tert*-butanol molecules between the volume and the surface was not observed (*28*), possibly because the *tert*-butanol was at a temperature only a little above its melting point (25.5°C) during imaging.

In order to observe surface ion absorption (relevant to ion exchange), we imaged the crystal surface under an ionic solution. The crystal was first washed with deionized water, and then a 0.1*M* aqueous solution of *tert*-butyl ammonium chloride was injected into the sealed cell of the AFM. The AFM image of the crystal surface in the *tert*-butyl ammonium solution is shown in Fig. 2D. Note that *tert*-butyl ammonium cations clustered on the surface of the crystal. These clusters of about 2 nm by 3 nm by 0.6 nm formed within ~1 min after the *tert*-butyl ammonium solution was injected. The clustering is probably due to the hydrophobicity of the apolar part of the *tert*-butyl ammonium ions (*25*).

It should be noted that because the microscope can begin imaging almost immediately after a fluid is injected into the cell, the adsorption of *tert*-butyl ammonium cations, that is, the growth of clusters, was observed in real time.

After imaging the surface in the *tert*-butyl ammonium solution, the clustering was then completely removed by rinsing the crystal with water without removing it from the AFM. Growths of new clusters were then

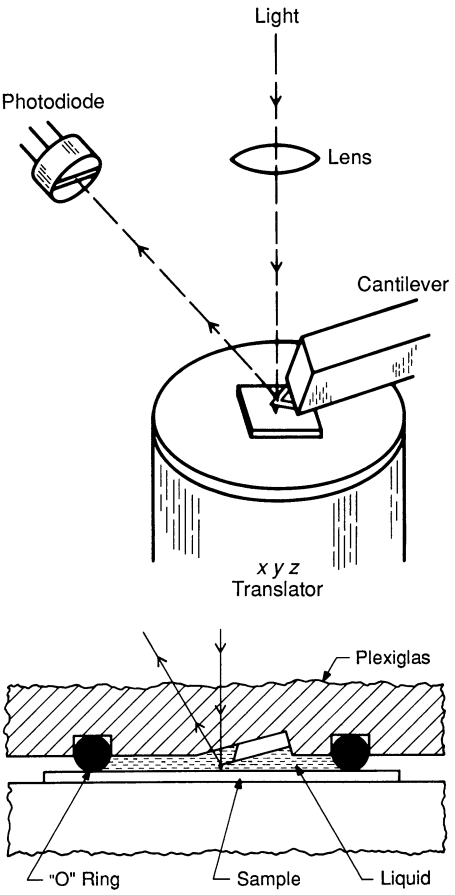

Fig. 1. AFM schematic. The AFM detects the vertical motion of the tip by sensing the displacement of the reflected beam with a two-segment photodiode (*10, 30*). A feedback loop keeps the vertical deflection of the tip, and therefore the force that the tip applies on the surface, constant by moving the surface up and down with the *xyz* translator. The imaging under liquid was performed with a sealed cell that is made of plexiglass and sealed with an O-ring. For more details, see (*17*).

A. L. Weisenhorn, S. A. C. Gould, P. K. Hansma, Department of Physics, University of California, Santa Barbara, CA 93106.
J. E. Mac Dougall, S. D. Cox, G. D. Stucky, Department of Chemistry, University of California, Santa Barbara, CA 93106.
W. S. Wise, Department of Geological Sciences, University of California, Santa Barbara, CA 93106.
J. Massie, P. Maivald, V. B. Elings, Digital Instruments, Inc., Goleta, CA 93117.

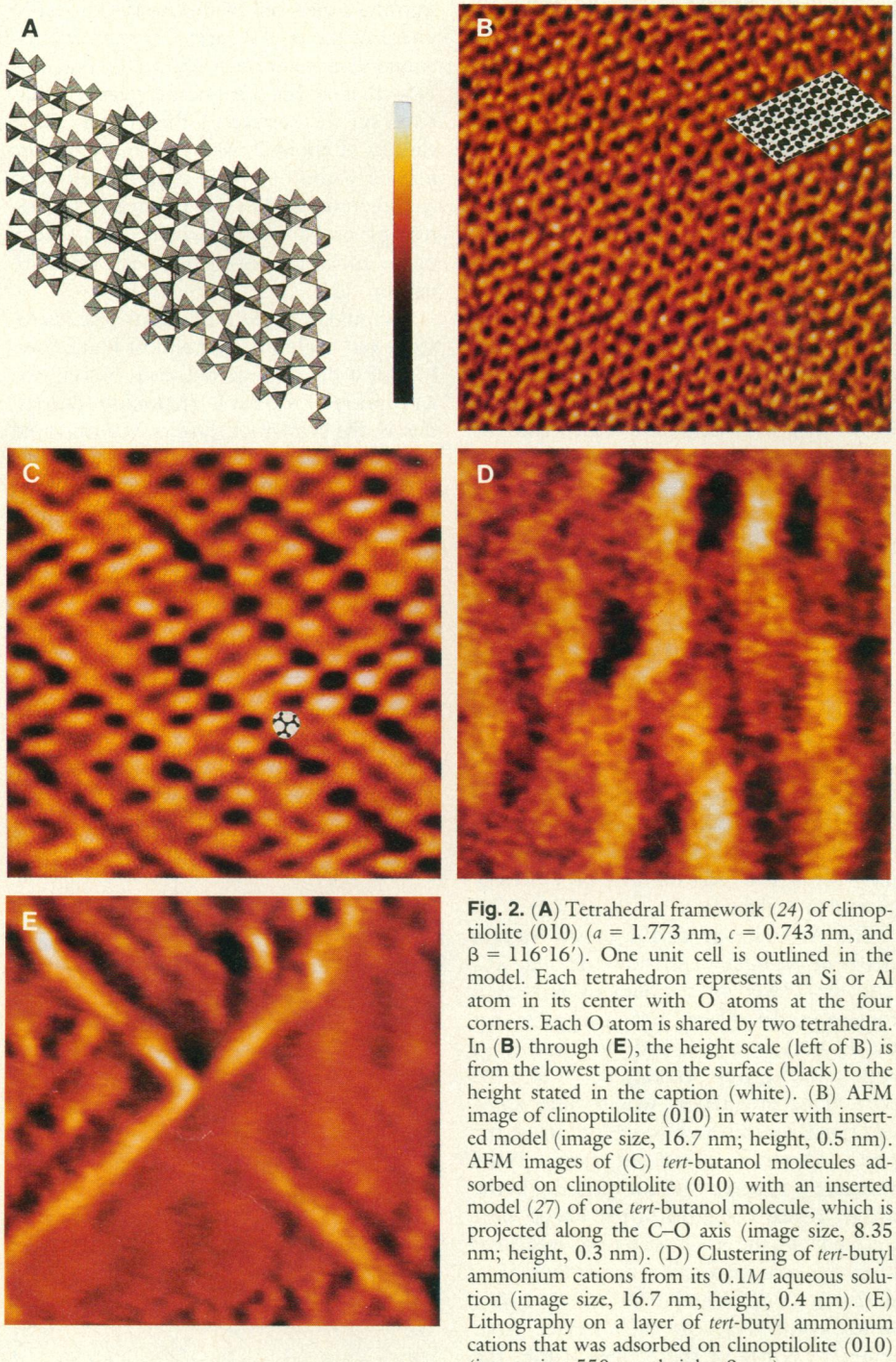

Fig. 2. (**A**) Tetrahedral framework (*24*) of clinoptilolite (010) (a = 1.773 nm, c = 0.743 nm, and β = 116°16′). One unit cell is outlined in the model. Each tetrahedron represents an Si or Al atom in its center with O atoms at the four corners. Each O atom is shared by two tetrahedra. In (**B**) through (**E**), the height scale (left of B) is from the lowest point on the surface (black) to the height stated in the caption (white). (B) AFM image of clinoptilolite (010) in water with inserted model (image size, 16.7 nm; height, 0.5 nm). AFM images of (C) *tert*-butanol molecules adsorbed on clinoptilolite (010) with an inserted model (*27*) of one *tert*-butanol molecule, which is projected along the C–O axis (image size, 8.35 nm; height, 0.3 nm). (D) Clustering of *tert*-butyl ammonium cations from its 0.1*M* aqueous solution (image size, 16.7 nm, height, 0.4 nm). (E) Lithography on a layer of *tert*-butyl ammonium cations that was adsorbed on clinoptilolite (010) (image size, 550 nm; height, 8 nm).

imaged after reintroducing *tert*-butyl ammonium solution. This process of adsorption and removal of clusters proved to be reproducible and reversible over several cycles. The observation of different absorption states (ordered arrays versus clusters) for different states of the molecule (neutral versus charged) is further confirmation that the AFM can nondestructively image adsorbed molecules.

Our final figure is from our investigation of lithography on the crystal surface. A layer of *tert*-butyl ammonium cations was adsorbed onto a clinoptilolite crystal, into which a cross "x" was "written" (Fig. 2E). The two crossing lines were scanned with a force greater than 10^{-8} N while simultaneously oscillating the crystal up and down at a frequency of ~5 kHz, which was achieved by increasing the proportional gain of the feedback loop. The "x" was imaged by scanning with a force smaller than 10^{-9} N. There were no detectable changes in the "x" or its environment during the 45 min in which it was monitored.

The monitoring as well as writing (removing) of molecules at active sites could form the basis of a new generation of biosensors. The biosensor would consist of an array of receptor molecules which would be continuously monitored to see if they had adsorbed any molecules. The surface could be periodically refreshed by having adsorbed molecules removed either by washing, chemical reactions, or by physically removing them with the AFM tip.

The AFM can be used to image zeolite surfaces with molecular resolution. With a sealed cell, real-time adsorption and clustering of molecules out of a liquid can be observed. Many important aspects of zeolite chemistry can be explored, such as sieving, external versus internal surface chemistry, and surface structural elucidation. In preliminary work on other zeolites, we have imaged the lattices of faujasite, scolecite, sodalite, and stilbite (*29*). Manipulating molecules on a zeolite surface opens up new and interesting possibilities for lithography and biosensors.

REFERENCES AND NOTES

1. For an introduction to zeolites, see D. W. Breck, *Zeolite Molecular Sieves* (Wiley, New York, 1974).
2. For a recent review, see C. J. Groenenboom, in *Zeolites as Catalysts, Sorbents and Detergent Builders*, H. G. Krage and J. Weitkamp, Eds. (Elsevier, New York, 1989), pp. 99–113.
3. See, for example, M. N. Harandi, V. M. R. Woen, G. P. McLaughlin, *Energy Fuels* **3**, 620 (1989).
4. R. M. Wise, European patent #EP 50894 (1984).
5. J. Olah, J. Papp, A. Mesazaros-Kis, Gy. Musci, D. Kallo, in *Zeolites as Catalysts, Sorbents and Detergent Builders*, H. G. Krage and J. Weitkamp, Eds. (Elsevier, New York, 1989), pp. 711–719.
6. For a recent review of zeolite science, see W. H. Flank and T. E. Whyte, Jr., Eds. *Perspectives in Molecular Sieve Science*, vol. 368 of the *ACS Symposium Series* (American Chemical Society, Washington, DC, 1988).
7. G. Binnig, C. F. Quate, Ch. Gerber, *Phys. Rev. Lett.* **12**, 930 (1986).
8. G. Binnig, Ch. Gerber, E. Stoll, T. R. Albrecht, C. F. Quate, *Europhys. Lett.* **3**, 1281 (1987); T. R. Albrecht and C. F. Quate, *J. Appl. Phys.* **62**, 2599 (1987); O. Marti, B. Drake, S. A. C. Gould, P. K. Hansma, *J. Vac. Sci. Tech. A* **6**, 287 (1988); P. K. Hansma, V. B. Elings, O. Marti, C. E. Bracker, *Science* **242**, 209 (1988).
9. M. D. Kirk, T. Albrecht, C. F. Quate, *Rev. Sci. Instrum.* **59**, 833 (1988).
10. G. Meyer and N. M. Amer, *Appl. Phys. Lett.* **53**, 1045 (1988).
11. T. R. Albrecht *et al.*, *J. Appl. Phys.* **64**, 1178 (1988).
12. S. A. C. Gould *et al.*, *Nature* **332**, 332 (1988).
13. D. Rugar, H. J. Mamin, R. Erlandson, J. E. Stern, B. D. Terris, *Rev. Sci. Instrum.* **59**, 2337 (1988); H. J. Mamin, D. Rugar, J. E. Stern, B. D. Terris, S. E. Lambert, *Appl. Phys. Lett.* **53**, 1563 (1988).
14. R. Erlandson, G. M. McClelland, C. M. Mate, S. Chiang, *J. Vac. Sci. Technol. A* **6**, 266 (1988); C. M. Mate, G. M. McClelland, R. Erlandson, S. Chiang, *Phys. Rev. Lett.* **59**, 1942 (1987).
15. J. E. Stern, B. D. Terris, H. J. Mamin, D. Rugar, *Appl. Phys. Lett.* **53**, 2717 (1988).
16. S. A. C. Gould *et al.*, *J. Vac. Sci. Technol. A* **8**, 369 (1990).
17. B. Drake *et al.*, *Science* **243**, 1586 (1989).
18. O. Marti, B. Drake, P. K. Hansma, *Appl. Phys. Lett.* **51**, 484 (1987).
19. A. L. Weisenhorn, P. K. Hansma, T. R. Albrecht, C. F. Quate, *ibid.* **54**, 2651 (1989).
20. Verification of the identity of the zeolite material from Succor Creek locality is based on x-ray powder diffraction and electron microprobe data (W. S. Wise, unpublished data).

21. Digital Instruments, Inc., 6780 Cortona Drive, Goleta, CA 93117.
22. K. Sugiyama and Y. Takeuchi, in *New Developments in Zeolite Science and Technology*, Y. Murakami, A. Iijima, J. W. Ward, Eds. (Elsevier, New York, 1986), pp. 449–456; A. B. Merkle and M. Blaughter, *Am. Min.* **42**, 273 (1967).
23. Note that clinoptilolite and heulandite are isostructural with different Si:Al ratios.
24. R. X. Fischer, *J. Appl. Crystallogr.* **18**, 258 (1985).
25. C. A. Bunton, private communication.
26. Fisher Scientific, Springfield, NJ.
27. Chemx, Chemical Design Ltd., Oxford, U.K.
28. J. D. Andrade, private communication.
29. J. E. Mac Dougall *et al.*, unpublished results. Manuscript in preparation.
30. N. M. Amer and G. Meyer, *Bull. Am. Phys. Soc.* **33**, 319 (1988); S. Alexander *et al.*, *J. Appl. Phys.* **65**, 164 (1989).
31. We thank R. van Ballmoos, D. H. Olson, R. B. Higgins, and M. Davis for helpful discussions, J. D. Andrade and H. E. Gaub for helping us see the possibilities for biosensors, G. L. Kelderman and T. Korda for technical support, and J. Gurley of Digital Instruments for his generous support with advice, electronics, and software. The Department of Geological Sciences provided the clinoptilolite crystals from their collection. Supported by an IBM Manufacturing Fellowship (A.L.W.), National Science Foundation–Solid State Physics grant no. DMR86-13486 (A.L.W., S.A.C.G., and P.K.H.), the Office of Naval Research (G.D.S. and P.K.H.), and E. I. duPont de Nemours & Co (G.D.S.).

26 December 1989; accepted 29 January 1990

Molecular Cloning of the *Bombyx mori* Prothoracicotropic Hormone

Atsushi Kawakami, Hiroshi Kataoka, Tadanori Oka, Akira Mizoguchi, Mina Kimura-Kawakami, Takashi Adachi, Masafumi Iwami, Hiromichi Nagasawa, Akinori Suzuki, Hironori Ishizaki*

Prothoracicotropic hormone (PTTH), a brain secretory polypeptide of insects, stimulates the prothoracic glands to produce and release ecdysone, the steroid essential to insect development. The complementary DNAs encoding PTTH of the silkmoth *Bombyx mori* were cloned and characterized, and the complete amino acid sequence was deduced. The data indicated that PTTH is first synthesized as a 224–amino acid polypeptide precursor containing three proteolytic cleavage signals. The carboxyl-terminal component (109 amino acids) that follows the last cleavage signal represents one PTTH subunit. Two PTTH subunits are linked together by disulfide bonds, before or after cleavage from prepro-PTTH, to form a homodimeric PTTH. When introduced into *Escherichia coli* cells, the complementary DNA directed the expression of an active substance that was functionally indistinguishable from natural PTTH. In situ hybridization showed the localization of the prepro-PTTH mRNA to two dorsolateral neurosecretory cells of the *Bombyx* brain.

Ecdysone, the steroid secreted by the prothoracic glands, is required for insect growth, molting, and metamorphosis. The prothoracicotropic hormone (PTTH), a brain neuropeptide, stimulates the prothoracic glands to synthesize and release ecdysone, thereby playing a central role in the endocrine network that controls insect development (*1*). Many efforts have been made to purify this hormone from insects (*1*), but purification has been hampered by the small amount present in the brain and by attendant technical difficulties inherent in protein purification. We previously isolated PTTH from the silkmoth *Bombyx mori* and determined the sequence of 13 amino acids from its NH_2-terminus (*2*). We then purified *Bombyx* PTTH on a far larger scale, concluded that PTTH is a dimeric molecule of relative molecular mass ~30 kD consisting of two identical or very similar subunits which are held together by one or more disulfide bonds, and sequenced the 104 amino acid residues from the NH_2-terminus of the subunit (*3*). The complete sequence was still unknown, however. Here, we report the cloning and characterization of the *Bombyx* cDNA which enabled us to deduce the complete amino acid sequence of PTTH.

By screening a *Bombyx* brain cDNA expression library with a mouse antiserum to PTTH (*4*) and then with an isolated positive clone as a hybridization probe (*5*), we obtained seven PTTH cDNA clones and characterized two types of cDNAs that encode prepro-PTTH, a precursor molecule for PTTH. The P-1 type cDNA contains an open reading frame that encodes a prepro-PTTH of 224 amino acids (molecular mass 26,027) consisting of a putative signal peptide segment containing the signal peptide (29 amino acids), two peptide components tentatively referred to as p2K (21 amino acids) and p6K (57 amino acids), and a PTTH subunit (109 amino acids), in this order from the 5′ end (Fig. 1). Proteolytic cleavage signals bound these components, suggesting that they are separated after translation. We defined the last component as the PTTH subunit because the amino acid sequence of this component up to the 104th residue matched the sequence determined by amino acid sequencing of purified PTTH (*3*), except for the 41st residue, which had not been identified because no phenylthiohydantoin derivatives of amino acids were detected at this cycle of Edman degradation. The 41st residue has now been deduced to be Asn, forming a possible N-linked glycosylation site together with the following two residues (Asn-Lys-Thr). The identification of this glycosylation site agrees with the previous evidence that *Bombyx* PTTH is a glycoprotein (*6*). The calculated molecular mass of the PTTH subunit (12,737) is slightly less than half the apparent molecular mass of purified mature PTTH [molecular mass of *Bombyx* PTTH has been estimated to be 22 kD by molecular sieving (*2*), but is now considered to be 30 kD from SDS electrophoresis data (*3*)]. The sequence length of the prepro-PTTH cDNA is consistent with the brain mRNA size of ~1.0 to 1.2 kb as determined by RNA (Northern) hybridization analysis (*7*). From these results and the previous amino acid sequencing data, we conclude that PTTH is first synthesized as a 224–amino acid polypeptide precursor containing a 109–amino acid PTTH subunit, and then two PTTH subunits are linked by disulfide bonds and glycosylated before or after posttranslational cleavage to generate a homodimeric mature PTTH. Sites of disulfide bonds remain to be determined. Peptide analysis of native PTTH (*3*) disclosed heterogeneity with respect to the chain length at the NH_2-terminus of the PTTH subunit, and possibly at the COOH-terminus also. This heterogeneity may be due to proteolysis during purification, posttranslational deletion of the terminal regions, or the presence of multiple PTTH genes differing in sequence. Two peptide components contained in prepro-PTTH, p2K and p6K, are presumed to be cleaved posttranslationally and may play some unknown physiologically or developmentally important functions.

A. Kawakami, T. Oka, A. Mizoguchi, M. Kimura-Kawakami, T. Adachi, M. Iwami, H. Ishizaki, Department of Biology, School of Science, Nagoya University, Nagoya 464-01, Japan.
H. Kataoka, H. Nagasawa, A. Suzuki, Department of Agricultural Chemistry, Faculty of Agriculture, The University of Tokyo, Tokyo 113, Japan.

*To whom correspondence should be addressed.